Environ Earth Sci (2010) 60:1245–1256
DOI 10.1007/s12665-009-0265-4

ORIGINAL ARTICLE

Identification of cross-valley faults in the Maynardville Limestone, Oak Ridge Reservation, Tennessee, using seismic refraction tomography

Shashank R. Atre · Philip J. Carpenter

Received: 20 November 2008 / Accepted: 28 July 2009 / Published online: 21 August 2009

Abstract First arrival times from P-wave refraction and reflection seismic surveys along Bear Creek Valley on the Oak Ridge Reservation, Tennessee, were inverted to produce refraction tomographic velocity images showing seismic velocity variations within thinly mantled karstic bedrock to a depth of approximately 20 m. Inverted velocities are consistent with two distinct bedrock groups: the Nolichucky Shale (2,730–5,150 m/s) and Maynardville Limestone (3,940–7,575 m/s). Low-velocity zones (2,700–4,000 m/s) in the tomographic images correspond to previously inferred cross-valley strike-slip faults; in places, these faults create permeability barriers that offset or block groundwater flowing along Bear Creek Valley. These faults may also force groundwater contaminants, such as dense non-aqueous phase liquids, to migrate laterally or downward, spreading contamination throughout the groundwater system. Other, previously unmapped cross-valley faults may also be visible in the tomographic images. Borehole logs suggest the low-velocity values are caused by low rigidity fractured and vuggy rock, water zones, cavities and collapse features. Surface streams, including Bear Creek, tend to lie directly above these low-velocity zones, suggesting fault and fracture control of surface drainage, in addition to the subsurface flow system. In some cases, fault zones are also associated with bedrock depressions and thicker accumulations of unconsolidated sediment.

Keywords Karst · Geophysics · Refraction tomography · Oak Ridge · Fractures

Introduction

Cross-valley faults and fractures in the Valley and Ridge province of the southern Appalachian Mountains complicate groundwater flow and contaminant migration as contaminants may migrate laterally from one set of strike-parallel flow zones to another. In many areas, cross-valley faults are also often overlain and obscured by meters or tens of meters of sediment. This study tests one geophysical method, seismic refraction tomography, as a means of imaging these cross-valley structures buried beneath 3–10 m of unconsolidated sediment.

Previous use of refraction tomography in karst areas

Applying seismic refraction tomography to near-surface targets (upper 30 m) is a relatively recent development in geophysics. The earliest papers employed refraction tomography for static corrections on seismic reflection surveys, not necessarily related to karst (e.g. De Amorim et al. 1987; Docherty 1992; Zhu et al. 1992). Belfer et al. (1998) combined refraction tomography, conventional intercept-time analysis and diffraction stacking to identify karst features and tunnels in Israel. Leucci (2003, 2004)

S. R. Atre
The Division of Sciences and Humanities,
Robert Morris University, 60085 Waukegan, IL, USA
e-mail: satre@robertmorris.edu

P. J. Carpenter (✉)
Department of Geology and Environmental Geosciences,
Northern Illinois University, 312 Davis Hall DeKalb,
60115 De Kalb, IL, USA
e-mail: pjcarpenter@niu.edu

integrated refraction tomography, electrical resistivity tomography and ground-penetrating radar to identify caves containing archeological artifacts in southern Italy, as well as mapping shallow karst aquifers and assessing their exposure to contamination. Carpenter et al. (2003) used seismic refraction tomography to image subcropping karstic bedrock in Kentucky and Illinois, and to identify depressions related to filled sinkholes and fractures. Although different tomographic inversion codes produced generally similar images of the buried bedrock, the bedrock surface in tomographic models was typically deeper than bedrock reported in borings, which often rely on auger refusal to identify the top of bedrock. Sheehan et al. (2005) conducted a comprehensive evaluation of three seismic refraction tomography codes, Rayfract™, SeisImager™ and GeoCT-II™, for eight typical subsurface karst features, ranging from a simple layered model to smallscale epikarstal pinnacles and caves. They concluded that artifacts resulting from lack of ray coverage are common in refraction tomographic images—smoothing the final model is necessary to eliminate these computational artifacts, but oversmoothing may remove legitimate features. They also suggest, if possible, forward modeling be used to validate refraction tomographic imaging of significant karst features. In a recent study Higuera-Diaz et al. (2007) used refraction tomography to identify a line of filled sinkholes associated with a major fracture at the Ft. Campbell Army Airfield in western Kentucky. These sinkholes are hydraulically connected and form a subsurface conduit for contaminant migration.

Geological and hydrogeological setting

This study was conducted near the Y-12 Plant within the Oak Ridge Reservation, Tennessee. The Oak Ridge Reservation is located in the Valley and Ridge province of the southeastern Appalachian Mountains and contains three national laboratory facilities: the Oak Ridge National Laboratory, the Y-12 and K-25 Plants. Figure 1 is a generalized map of the reservation showing the study site located in Bear Creek Valley, approximately 5-km southwest of the main portion of the Y-12 Plant. A detailed map of the study area is shown in Fig. 2.

Geological setting

Bear Creek Valley lies on the Whiteoak Mountain thrust sheet which contains numerous geological structures on several scales. The Valley is underlain by southeast-dipping Maynardville Limestone and Nolichucky Shale, both of Upper Cambrian age (Table 1). Cambrian Copper Ridge Dolomite (Knox Group) outcrops on ridges surrounding Bear Creek Valley. The contact of the Maynardville Limestone and Nolichucky Shale, both members of the Conasauga Group, runs parallel to and about 100-m northwest of Bear Creek (Hatcher et al. 1992). These rocks, which strike between N47°E and N67°E, have an average dip of 43° to the southeast (King and Haase 1987; Hatcher et al. 1992).

Fractures and faults are particularly important because these largely control groundwater flow in Bear Creek

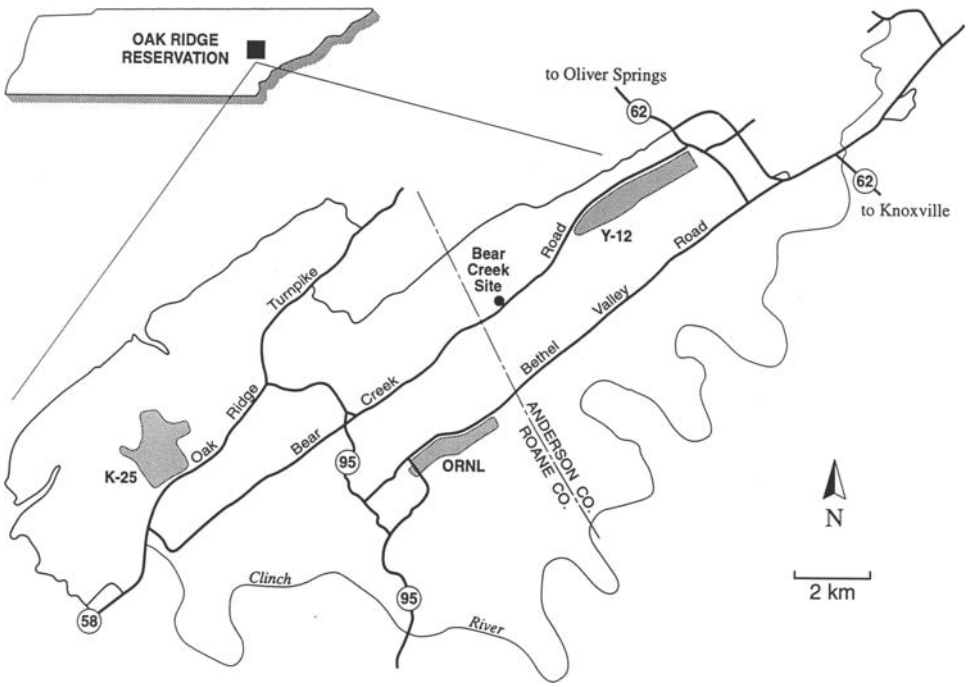

Fig. 1 A generalized map of Oak Ridge Reservation showing the study site and its location in the state of Tennessee, USA (after Carpenter et al. 1998). Bear Creek Road runs along the bottom of Bear Creek Valley. The "Bear Creek Site" is the study area

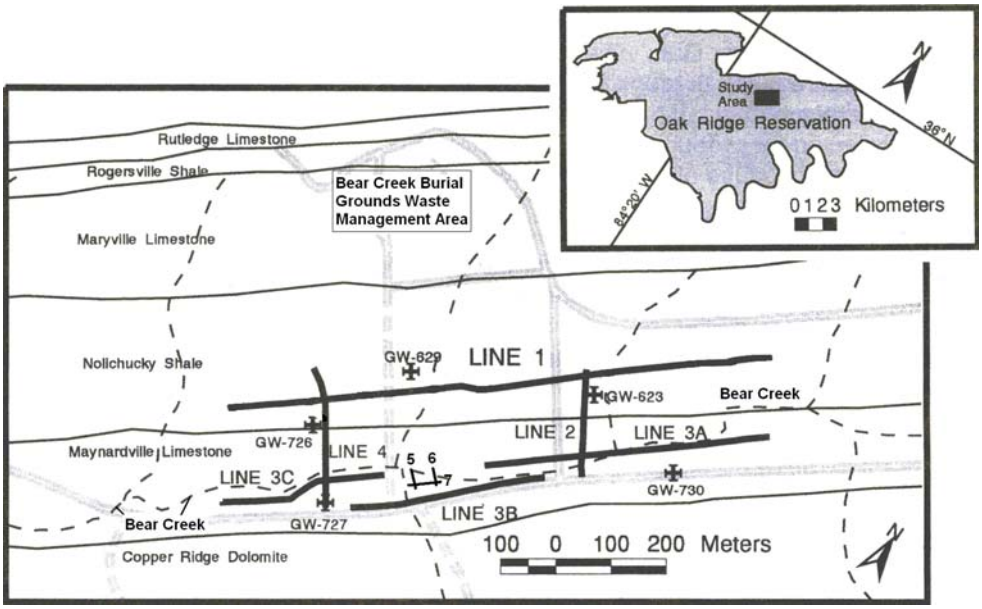

Fig. 2 The seismic refraction lines used in this study, along with approximate buried contacts. Roads and major streams are shown as *dashed lines* (after Doll 1998). A few of the wells used in this study are also shown

Valley. Several systematic joint sets in Bear Creek Valley have been identified by Foreman and Dunne (1991) and Hatcher et al. (1992). These include bedding plane fractures that strike approximately N55°E and dip approximately 45° to the southeast, bedding-perpendicular strike-parallel joints that strike approximately N41°E, dipping 45° to the northwest, and other joint sets that strike obliquely (N15°E and E–W) or at high angles to the strike of the formations, including those joints trending approximately perpendicular to strike (N54°W, dip 54°SW).

The latter joint sets have trends consistent with "cross-valley" faults discovered by Hollon (1997), who noted in core samples lateral and vertical offsets in subunits of the Nolichucky Shale. The presence of Hollon's cross-valley faults is supported by apparent faults dipping 54°–60° on a seismic reflection section (Doll 1998), and lineaments visible on aerial photos of Bear Creek Valley. Hollon estimated the maximum horizontal offset along these faults as 50 m; the vertical offset is probably <10 m. Figure 3 shows a map with Hollon's six cross-valley faults (labeled H1–H6) as well as Hollon's interpreted displacement of the Maynardville Limestone, and the seismic lines used in this study.

Hydrogeology

The hydrogeology of the Oak Ridge Reservation, and Bear Creek Valley in particular, are discussed extensively in Moore (1988); Solomon et al. (1992), Shevenell et al. (1992); Shevenell and Beauchamp (1994) and Goldstrand and Shevenell (1997). Most groundwater on the reservation is produced from the Knox aquifer, which consists of several formations, as shown in Table 1. One of these formations is the Maynardville Limestone, which averages 76 m in thickness, and subcrops beneath 3–10 m of alluvium along most of the length of Bear Creek Valley. Potentiometric levels in the study area suggest overall groundwater flow is to the southwest, along the valley and parallel to the strike of the Maynardville Limestone. A strong interconnection exists between Bear Creek, other surface streams, and the groundwater system (Geraghty et al. 1985).

Porosity and permeability of the Maynardville Limestone

Porosity development in the Maynardville Limestone is discussed extensively by Dreier et al. (1987), Goldstrand (1995), and Goldstrand and Shevenell (1997). Matrix porosities range from 0.5 to 2.1% in the Maynardville; this porosity apparently results from the dissolution of gypsum, anhydrite, carbonate mudstone and pyrite, as well as dedolomitization. Slow matrix flow accounts for about 32% of the water-producing intervals in Bear Creek Valley. Hydraulic conductivities as small as 0.12 m/day have been measured in these zones.

Fracture porosity and karst conduits (cavities and solutionally enlarged fractures with apertures greater than 6 cm) account for 68% of the water-producing zones in the Maynardville. In general, the number of fractures and spacing between fractures decreases with depth; fracture spacing also increases with bed thickness (Sledz and Huff 1981; Moore 1988). Cavities and karst conduit flow are concentrated in the upper 35 m. Below this depth, fractures and matrix porosity probably convey most groundwater. Most cavities encountered during drilling are

Table 1 Geologic units within Bear Creek Valley

Unit	Age	Thickness (m)	Dominant lithology
Rockwood Formation	Silurian	120	Sandstone, shale
Sequatchie Formation	U. Ordovician	60	Argillaceous limestone
Reedsville Shale	U. Ordovician	60	Calcareous shale
Chickamauga Group	M. Ordovician	400–700	Limestone, argillaceous limestone, shale, siltstone
Knox Group	Lower Ordovician/Upper Cambrian	75–120	Massive dolomite, siliceous dolomite, bedded chert, limestone, some clastics
Mascot Dolomite			
Kingsport Formation		90–150	
Longview Dolomite		40–60	
Chepultepec Dolomite		150–215	
Copper ridge Dolomite		245–335	
Conasauga Group	Middle, Upper Cambrian	125–145	Dolomitic limestone, limestone, shale, siltstone, calcareous siltstone and shale, shaly limestone, limestone
Maynardville Limestone			
Nolichucky Shale		100–150	
Dismal Gap Formation (formerly Maryville Limestone)		95–120	
Rogersville Shale		20–35	
Rutledge Limestone		30–40	
Pumpkin Valley Shale		90–100	
Rome Formation	Lower Cambrian	90–125	Shale, siltstone, sandstone, local dolomite lenses

Knox aquifer units are in italics

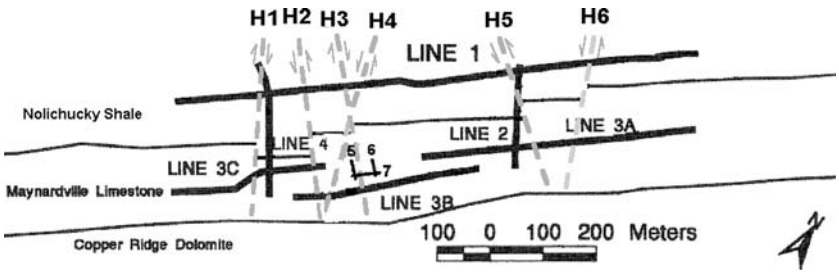

Fig. 3 Seismic refraction lines in relation to strike-slip cross-valley faults proposed by Hollon (1997) (adapted from Doll 1998). The *dashed gray lines* represent Hollon's cross-valley faults

solution-enlarged bedding planes, and occur where the bedding intersects other joints and faults. Minor thrust faults (duplicating 3- to 6-m sections of strata) have also been observed in core; inter-well connections verify that these faults also function as karst conduits (Goldstrand and Shevenell 1997).

According to Hollon (1997), the cross-valley strike-slip faults, which are the focus of this investigation, acutely influence groundwater flow in Bear Creek Valley. Strike-parallel flow along interconnected fractures, karst conduits and thrust faults may be interrupted by faulted low-permeability shale beds. This causes groundwater (and any entrained contaminants) to migrate along the fault plane until it finds another high permeability strike-parallel zone. Hollon (1997) also notes that these cross-valley structures affect "the hydraulic gradient by increasing the ground water potentiometric head, because cross-fault permeability is less than that of adjacent laterally permeable zones."

Groundwater contamination in Bear Creek Valley

At the Bear Creek Burial Grounds, chemical and radioactive wastes were commonly disposed of in unlined trenches, holes and lagoons from 1955 until 1981. In 1990, dense non-aqueous phase liquids (DNAPLs) were detected at a depth of 84 m along the southern edge of the Bear Creek Burial Grounds (Fig. 2). Dissolved phase contaminants have since been detected in wells within the Nolichucky Shale bordering the Maynardville Limestone. The presence of DNAPL at increasing depth parallel to the

regional dip direction suggests DNAPLs may have migrated along a particular stratigraphic horizon, or along a strata-bound fracture or fault zone (Dreier and Caldanaro 1994). DNAPLs from the Bear Creek Burial Grounds thus appear to be moving downdip to the southeast, while simultaneously migrating down valley, to the southwest. In this model, when the DNAPL encounters a cross-valley strike-slip fault, the free-product portion sinks several tens of meters, looking for another highly conductive zone. The dissolved phase, however, probably remains in the groundwater, spreading laterally (Hollon 1997). King and Haase (1987) suggest fractures within the Nolichucky are connected to solutionally enlarged fractures in the Maynardville and that once dissolved phase contaminants enter the karstic Maynardville they may be quickly conveyed offsite.

Data collection, processing and analysis

Previous seismic studies in Bear Creek Valley

Doll (1998) describes a series of seismic reflection experiments and surveys in Bear Creek Valley utilizing data collected by the Kansas Geological Survey during the summer of 1992. Forty-eight channel common-midpoint (CMP) gathers were recorded from an auger-gun source. Geophone groups were spaced 3-m apart with each group consisting of 3 Mark Products L-28E 40 Hz geophones, each separated by 0.3 m connected in series. A 48-channel EGG Geometrics 2401 seismograph was used to record the data. Seismic traces were collected with an "end-on" configuration in which the auger gun was usually offset 12 m from the nearest geophone group and 174 m from the furthest group. A few shots at each line were also made with smaller offsets to obtain data that could be used for static corrections. The auger gun was then moved into the line of geophones and occupied successive geophone positions. Geophones ahead of the source were turned on with a roll-along switch, so that the offsets from the shot remained constant along the recording geophones.

Static problems and surface waves severely degraded the data, and, initially, reflections could not be identified. After application of spectral balancing, refraction statics and common-midpoint stacking, reflections became visible along Line 1, over the Nolichucky Shale (Doll et al. 2005). This particular section was used by Hollon (1997) to image cross-valley faults H4 and H6, and to estimate their dips. Doll et al. (2005) notes that even with this advanced processing, however, reflections were non-existent or discontinuous over the Maynardville Limestone along Lines 2, 3, and 4. He attributed the poor data quality and lack of clear reflections to absorption of seismic energy in air-filled cavities and fractures, scattering from heterogeneities, extremely variable near-surface conditions, and other factors. In response to these problems, and similar lack of success with refraction methods that depend on layered earth models, Doll suggested seismic refraction tomography be employed in Bear Creek Valley to image the Maynardville Limestone.

In a much smaller-scale unrelated study, Chen et al. (2006) successfully jointly inverted crosshole seismic wave travel times and borehole flowmeter data to tomographically image fracture zones in the Nolichucky Shale at a bioremediation site in Bear Creek Valley. Low velocities corresponded to fractured zones and zones containing solution openings.

Seismic data for refraction tomography

First arrival times from data collected along seismic reflection Lines 1–4, as described above, were used in this study, in addition to arrival times from three shorter seismic refraction lines (Lines 5–7), as shown in Figs. 2 and 3. Lines 1–4 contain data collected in only one direction—i.e. the shot was not reversed since these were seismic reflection lines. Apparent dips in the resulting tomographic images from these lines should thus be regarded as superfluous, being strongly influenced by shot position.

Lines 5–7, however, were collected as refraction lines using a 5.5 kg sledgehammer source, one line of 48 geophones, with single geophones at 0.6 m intervals and multiple shotpoints, beyond both ends of the lines and within the lines. Lines 5–7 thus provide fully reversed refraction data sets with multiple source points. Lines 5–7 are much shorter than Lines 1–4, but they contain fully reversed data at many different offsets.

Data analysis

First-break times of direct and refracted P-wave arrivals were manually picked using the display software Seisx (Thompson 1995) and plotted on time–distance graphs. After an initial quality check and preliminary dipping layered model interpretation first arrival times for each line were input into the commercial refraction tomography software package, GEOCT-I™ (GeoTomo 2001), which inverts travel times to produce a two-dimensional (2D) velocity image of the subsurface.

GeoCT-I uses a non-linear least squares inversion process devised by Zhang et al. (1998), and a wavefront propagation approach, for the modeling of travel times. A unique aspect of GeoCT-I is that the inversion algorithm seeks to minimize the difference between data and model

values for both the average slowness (travel time divided by raypath length) and apparent slowness (slope of the travel time curve), instead of just minimizing the misfit between modeled and observed travel times. GeoCT-I also utilizes Tikhonov regularization to minimize model "roughness" (Zhang and Toksöz 1998).

Various tests were run in which model inversion parameters were varied and solution stability assessed. Different initial models were tested with <10 to over 20 inversion iterations. At large numbers of iterations, only minor changes occurred in the final model with dramatic increases in processing time. On the other hand, employing <10 iterations resulted in a model that is only moderately perturbed from the initial model, and the misfit is larger. Thus, 10 iterations were used for most refraction tomographic velocity inversions in this study.

Changing the smoothing (constraint) parameter moderates the degree of change from cell to cell. If the smoothing parameter is large, short-wavelength structures will be averaged and reduced (or disappear outright). On the other hand, when the smoothing parameter is set too small many short-wavelength artifacts appear. The default (moderate) smoothing constraint was chosen as a compromise between an overly smoothed versus artifact-laden tomographic image. Finally, different maximum and minimum velocity limits were tested for the inversions. The robustness of the velocity model was found to be dependent, for the most part, on the number of shot points, and the number and spacing of geophones in a spread. Large numbers of shot points, in which geophones have redundant coverage at different offsets, produce the most stable velocity models.

Element size varied from 0.7 m for the short lines to 9 m for the longest lines. The number of elements in the x (horizontal) direction was typically about 205 and the number of vertical elements was about 20 for most images. The limited processing capacity of GeoCT-I required that Line 1 be broken into three segments for inversion, and Lines 3a and 3b broken into two segments each. GeoCT-I also provides little control over how the sections may be plotted. Thus, the vertical exaggeration often varies between the refraction tomography sections. In the following sections, vertical exaggerations vary from a minimum of 3.1 (Line 7) to as much as 8.5 (Line 1). Faults and contacts thus appear much steeper than they actually are in nature.

Comparison with well logs and identification of units on the tomographic images

Numerous groundwater monitoring wells are present in this field area—many of these were within 30 m of the seismic lines and are shown in the images as projected well logs. Figure 4 shows the location of the groundwater monitoring wells, relative to the seismic lines. Although only a few of these wells have geophysical logs, all of them have drillers logs which provide depth to the top of bedrock, and in some cases depth to the top of both weathered and fresh bedrock, based on subjective interpretation by the driller (Betchel National, Inc. 1984a, b, c; Jones et al. 1992). Some of these wells also have information on depth to water horizons, water "breaks" and the depth to fractures and cavities. The water-level data, unfortunately, was not contemporaneous with the seismic studies. Also, substantially different water levels are often recorded for the same well over a span of just a few days. This information is displayed, where available, on the sections.

Individual velocity cells in the tomographic images were lumped into seven velocity groups shown in Table 2 to provide a consistent color scheme from image to image. These velocity groups are based on a comparison with the drillers logs and the few acoustic velocity logs made in the Maynardville Limestone on the Oak Ridge Reservation. Unsaturated sediments are represented by Units 1–2 (sandy brown to green). Units 2 and 3 (green and blue) are probably largely saturated, although it is likely that some of the water levels within Unit 2 represent water under perched or transient conditions, and should not be interpreted to mean the entire green unit is saturated. Unit 3 (blue) is more likely to represent fully saturated sediments, or compact rigid sediments. Unit 4 (silver-gray) probably represents highly weathered bedrock. Unit 5 (brown) may represent less weathered bedrock, and Units 6 (red) and 7 (dark blue) probably represent fresh bedrock. The top of Unit 5 was chosen as the top of bedrock and is highlighted with an undulating bold line in the refraction tomographic sections.

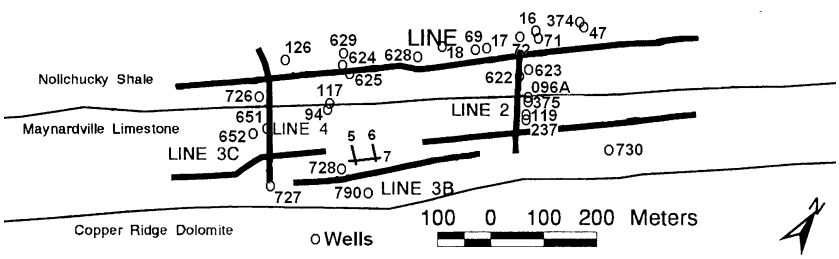

Fig. 4 Groundwater wells are shown with seismic refraction lines and approximate locations of buried contacts. The "GW" prefix is omitted from all well numbers to improve clarity (adapted from Doll 1998)

Table 2 Velocity units for tomography

Unit	Color	Velocity range (m/s)	Probable lithology
1	Sandy brown	300–850	Soil, relatively dry sediment
2	Green	850–1,490	Clayey or partially saturated sediment
3	Blue	1,490–2,000	Saturated or competent sediment
4	Silver-gray	2,000–2,730	Heavily weathered bedrock
5	Brown	2,730–3,940	Moderately weathered bedrock
6	Red	3,940–5,150	Unweathered Nolichucky Shale
7	Dark blue	5,150–7,575	Unweathered Maynardville Limestone

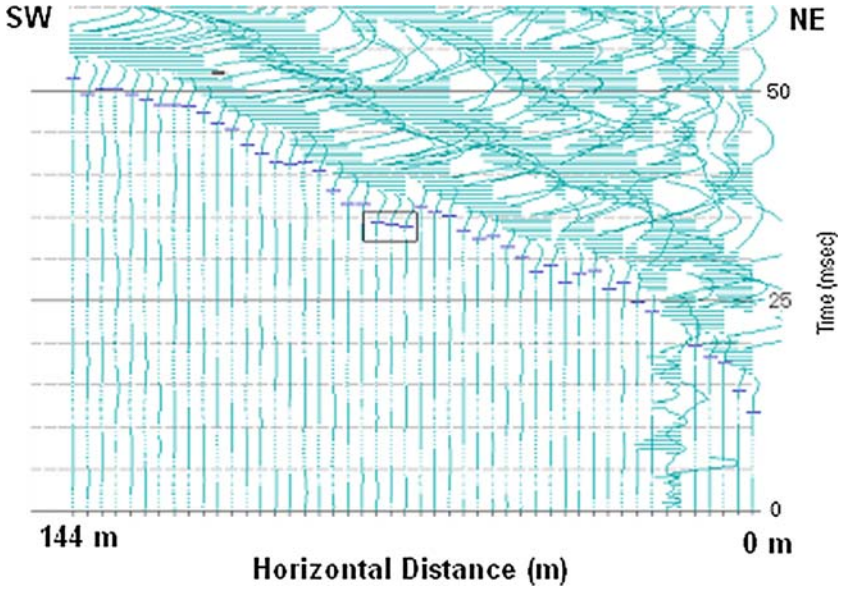

Fig. 5 Field record of a shot point on Line 1, Segment 1, at position 390 m. *Short horizontal dashes* indicate first-arrival picks. The shot is offset 12 m from the northeastern geophone group. Distances along the *bottom* represent distance from the first geophone, not the offset. Traces 25, 26, and 27 (*boxed*) show that the first arrivals from the bedrock refractor arrive earlier, and at much faster velocity, than adjoining traces

Results and discussion

In this section, seismic traces in the raw data are examined for congruence with the final tomographic models, and the imaging of gross changes in lithology is assessed. Imaging of previously inferred cross-valley faults is then described, along with the discovery of new faults.

Verification of tomographic models

Field record verification of refraction tomographic features

Field records were examined to assure features on the tomographic models were consistent with the field data. Figure 5 is a typical example of seismic traces from Line 1. The shotpoint is to the northeast, offset 12 m from the first geophone. P-wave first arrival picks (short horizontal dashes) indicate a heterogeneous subsurface. Decreased slopes of the first arrival P-waves, for example, within the box between traces #25–27, and changes in slope elsewhere on this field record, suggest the presence of abrupt velocity increases and decreases. This velocity increase (along with a similar flattening in the arrival times on adjacent field records) is responsible for the abrupt velocity increase (from red to blue) at about position 370 m, 18-m depth on the refraction tomographic image of Line 1, Segment 1, as shown in Fig. 6. Other examples of consistency testing between field records and final refraction tomographic images may be found in Atre (2006).

Imaging the Maynardville/Nolichucky contact

The major geologic contact between the Maynardville Limestone and Nolichucky Shale shows up well in the tomographic images (Fig. 7). The Maynardville exhibits a velocity in the range 3,940–7,575 m/s (red to dark blue), whereas the Nolichucky usually is slower, generally about 2,730–5,150 m/s (brown to red). The lower velocity Maynardville (which overlaps the Nolichucky velocity) probably represents weathered limestone along faults and fractures, or Maynardville near the top of the subcropping

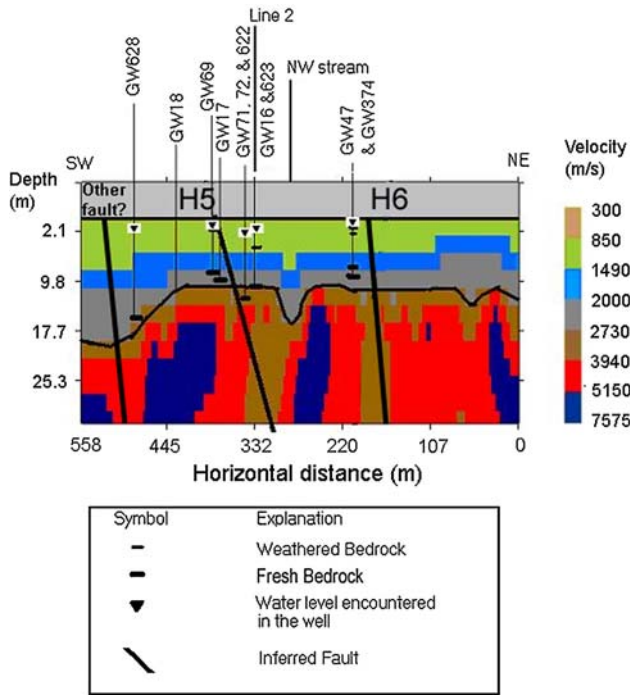

Fig. 6 Tomographic 2-D velocity model for Line 1, Segment 1. Inferred strike-slip faults from Hollon (1997) have been plotted. *Legend* shows symbols used in cross-sections, including symbols obtained from well logs. *Horizontal bold line* represents the Earth's surface and the *undulating bold line* deeper in the section represents the interpreted top of bedrock. Locations of streams are also noted on this and the following sections

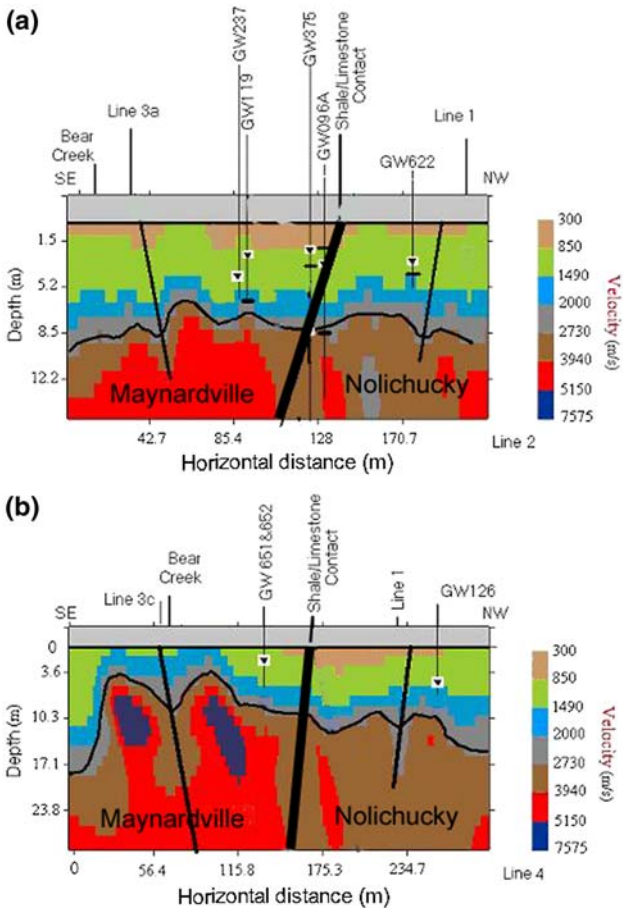

Fig. 7 Tomographic 2-D velocity models of Lines 2 and 4: **a** Line 2, and **b** Line 4. The geologic contact between Nolichucky Shale and Maynardville Limestone is shown as the *heavy bold line*—this contact is not a fault. *Legend* and *explanation* for other symbols may be found on Fig. 6

bedrock. These values are consistent with velocities recorded by sonic well logs in these formations (King and Haase 1987, 1988). Thus, the Maynardville clearly exhibits a higher velocity in both images, which suggests the refraction tomography is responding accurately to lithologic changes.

Another way gross changes may be evaluated is to compare refraction tomographic images from Line 1, such as in Fig. 6, which lies entirely over the Nolichucky, to that obtained over Line 3c, which lies entirely over the Maynardville Limestone (Fig. 8). With the exception of interpreted faults and fracture zones, the overall velocity shown in Fig. 8 is considerably higher than that visible in Fig. 6, reflecting the higher velocity of unweathered limestone compared with that of shale. Figure 6 suggests, however, that a few parts of the Nolichucky, where the dark blue patches appear, exhibit velocities similar to that of the Maynardville—perhaps these represent the carbonate subunits within the Nolichucky (Hatcher et al. 1992).

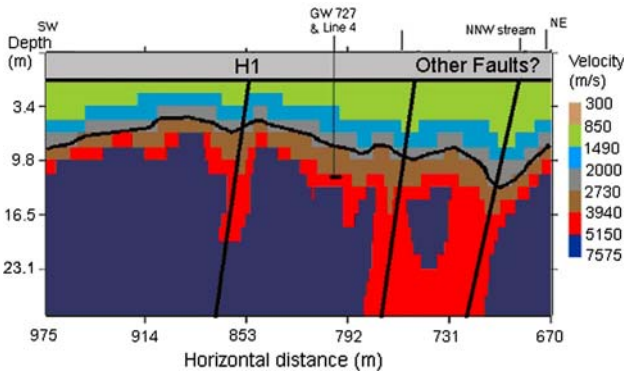

Fig. 8 Tomographic image of Line 3c (i.e. the southwest segment of Line 3) showing low-velocity zone near fault (H1) proposed by Hollon (1997), as well as two possible previously unidentified faults. *Legend* and *explanation* for symbols may be found on Fig. 6

Imaging cross-valley faults

Low-velocity zones in the refraction tomographic images have been annotated by heavy black lines on Figs. 6, 7, 8. These correspond to the cross-valley strike-slip faults proposed by Hollon (1997), as well as other possible faults. Those corresponding to Hollon's positions are labeled

H1–H6, as in Fig. 3; other faults inferred from the tomographic images are also depicted with heavy black lines, but are not numbered. Well logs from Jones et al. (1992) and Atre (2006) will be examined in detail below to see what features were encountered in borings near these fault zones. Well locations are plotted on the refraction tomography sections to assist in this discussion.

Faults along Line 1

Figure 6 show a section from Line 1. Well logs from Jones et al. (1992) indicate shale at the base of GW17, GW47, and GW374, which is consistent with the location of bedrock highs between the inferred fracture zones and faults. The log for GW16 lists no fractures or voids, despite its proximity to fault H5. However, the log for GW71 records a "water blowout" at 7.0-m depth, possibly due to a fracture zone associated with H5. The log for GW623 also records "fractures with water" at various depths. GW628, near the southwestern end of this segment, encountered a fracture zone and a thickening of unconsolidated overburden to about 18-m depth. A dark black line representing an inferred fault or unnamed fracture zone was thus added to the section in the interpreted bedrock depression near GW628. DNAPL was also encountered in this well at 82-m depth, far below the base of the refraction tomography section.

Faults along Lines 2 and 4

Figure 7 shows Lines 2 and 4, which both traverse Bear Creek. This section was discussed above in the context of refraction tomographic response to major lithologic change. These images are examined here for low-velocity zones that could be faults. Figure 7a and b suggests two additional unnamed faults or fracture zones trend along the axis of the valley, including a possible fault and low-velocity zone directly beneath Bear Creek. The log from GW119 records competent bedrock at about a depth of 6.8 m which is supported by the refraction tomographic image shown in Fig. 7a.

Faults along Line 3

Figure 8 depicts the southwestern segment of Line 3 (3c). The well log from GW727 records competent bedrock at a depth of 11.9 m, which is consistent with high velocity material indicated in the tomographic image of Line 3c (Fig. 8). The prominent red zone of slightly lower velocity at position 700–780 m may indicate yet other cross-valley faults or a fault zone. This zone appears to be a major low-velocity zone and is about 60-m wide.

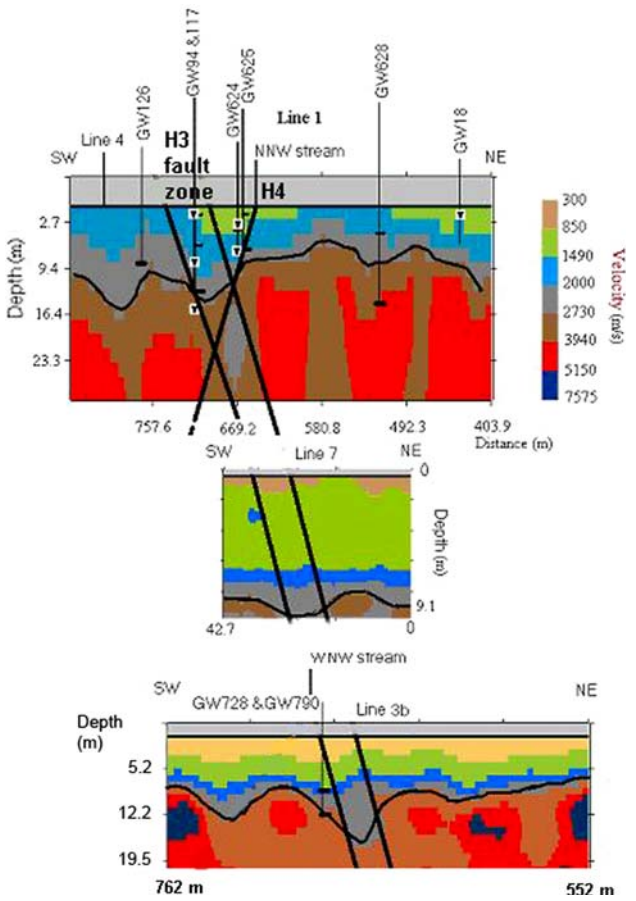

Fig. 9 Lines 1, 7 and 3, showing a wide strike-slip zone (H3) proposed by Hollon (1997). The *top* section is a portion of Line 1, Segment 2, the middle section is Line 7, and the bottom section is a portion of Line 3b. The *lines* are in correct lateral alignment, although the distances between the lines are compressed

The H3 fault zone

Line 1, Segment 2, Line 7 and Line 3b all show evidence of the H3 fault zone. Hollon (1997) suggests a wider area of fracturing for H3 than the other fault zones. This seems to be reflected in the refraction tomography images. Figure 9 shows all three refraction tomography sections aligned in their correct lateral positions. Fault zone H3 appears to be responsible for a low-velocity zone on Line 1, Segment 2 (top panel), and this fault zone appears to be coincident with thicker overburden and low-velocity zones along Lines 7 and 3b (middle and lower panels respectively). The top panel in Fig. 9 also suggests a heavily disturbed zone (represented by a wide low-velocity zone) at the intersection of faults H3 and H4. This is supported by the drillers logs from GW117 which has a zone of water inflow extending from 9.1 to 16.7 m depth—this is probably a solutionally enlarged fracture or fracture zone(s). Water levels (indicated by the inverted triangle symbols) in this disturbed zone also fluctuate greatly from well-to-well, or

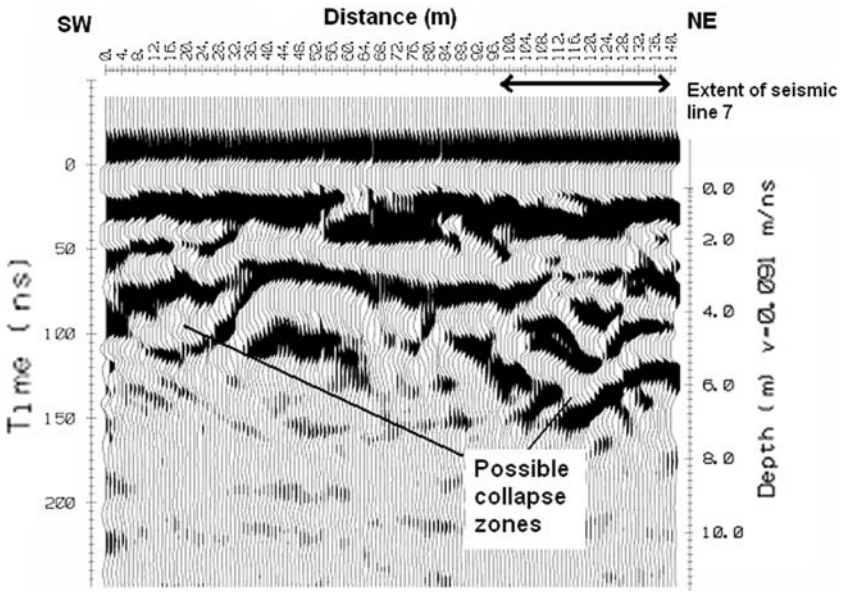

Fig. 10 Ground-penetrating (GPR) radar image from a profile that includes seismic Line 7 showing apparent collapse features along the H3 fault zone (after Carpenter et al. 1995). The extent of Line 7 on the GPR section is shown by the *arrows*

even within the same well, in a rather anomalous manner. Substantial fracturing has also been recorded in well GW625 near the H4 fault zone. On Line 3b (bottom panel of Fig. 9) logs from GW728 record silty and cherty "void fill" below 10-m depth and the log from GW-790 records fractures around 35-m depth. Both of these wells are adjacent to the H3 fault zone.

Finally, a ground-penetrating radar line coincident, in part, with seismic Line 7 suggests collapse features in this same area (Fig. 10). These collapse features may account for the thickening of the overburden along this fault zone, as suggested by Lines 7 and 3b.

Stream trends and underlying fracture zones

Surface streams, usually with northeast or northwest orientations, lie directly above low-velocity zones and inferred faults on several of the refraction tomography images. The location of these streams is noted at the top of the images in Figs. 6, 7, 8, 9. For example, a northwest-trending stream lies directly above the low-velocity trough between H5 and H6 in Fig. 6. Figure 7b (line 4) suggests a low-velocity zone lies directly beneath Bear Creek. A northwest-trending stream lies over the low-velocity zone near the northeast edge of Line 3c in Fig. 8. Finally, the top panel in Fig. 9 (Line 1, Segment 2) suggests a north–northwest trending stream lies directly over fault H4, whereas the bottom panel (Line 3b) suggests a west–northwest trending stream lies on the southwestern edge of the H3 fault zone. Thus, many of the streams in this portion of Bear Creek Valley may be fault or fracture controlled.

Conclusions

The following conclusions may be drawn from this study:

1. Refraction tomography velocity models effectively image low-velocity zones in the subsurface that probably correspond to faults and fractures. These discontinuities are important in structural geology, hydrogeology and engineering geology.
2. Refraction tomography may be able to provide subsurface images and models in karstic areas where conventional seismic refraction and reflection methods fail. Specifically, refraction tomography appears to be an effective tool for mapping lateral velocity discontinuities in the shallow subsurface and for mapping bedrock relief. The water table, or saturated sediments, may also be identified, in some cases.
3. Seismic reflection data sets may be "reused" for seismic refraction tomography. Although seismic reflection data is generally collected in a unidirectional mode, considerable information on the shallow subsurface exists within these data sets and may be extracted by inverting the first arrival times using refraction tomography.

Velocities of bedrock obtained through tomographic inversion are consistent with two distinct bedrock groups: the Nolichucky Shale (2,730–5,150 m/s) and Maynardville Limestone (3,940–7,575 m/s). Low-velocity zones (P-wave velocity of 2,700–4,000 m/s) in the refraction tomographic images correspond to previously inferred cross-valley strike-slip faults. Boreholes, and ground-penetrating radar sections, suggest the low-velocity values are caused by low

rigidity fractured and vuggy rock, water zones, cavities and collapse features.

Several other faults probably occur where steeply dipping low-velocity zones cut the tomographic images, in addition to the six previously inferred strike-slip faults. Surface streams, including Bear Creek, tend to lie directly above these low-velocity zones, suggesting fault and fracture control of the surface drainage. In some cases, fault zones are also associated with bedrock depressions and much thicker unconsolidated overburden.

Future surveys in Bear Creek Valley should concentrate on the cross-valley fault zones identified in this study. Fully reversed refraction surveys with shots within the lines, with a tight geophone spacing (about 0.3 m), would provide high-resolution tomographic images of the cross-valley fault zones without the distortions present in the unidirectional seismic reflection data set. Other geophysical methods (e.g. resistivity tomography) could also be employed over these fault zones. Finally, boreholes could be drilled in locations corresponding to the inferred "other faults" based on the refraction tomography images obtained here, to test the accuracy of these models. Ultimately, the conceptual groundwater flow and contaminant migration model for Bear Creek Valley will be refined by delineating these cross-valley faults.

Acknowledgments We thank and acknowledge Dr. William Doll and Stephen Fields of Oak Ridge National Laboratory, Tennessee, for providing the seismic and hydrogeological data that was used in this research project. We would also like to thank Dr. Mike Thompson of MDT Consultants, Bolingbrook, Illinois, who provided software for picking arrival times. The Department of Geology and Environmental Geosciences of Northern Illinois University also provided resources for the completion of this manuscript. Ms. Sandra Schramel of the Emergence Dance Theater of DeKalb also graciously provided working space where many hours were spent revising this manuscript while observing dance rehearsals. Finally, we are grateful for insightful and useful comments from an anonymous reviewer which greatly improved this manuscript.

References

Atre S (2006) Accuracy and reliability of tomographic 2-D seismic velocity models to map karst structures and infer hydrogeological processes in karst. PhD, Northern Illinois University, DeKalb, p 398

Belfer I, Bruner I, Keydar S, Kravtsov A, Landa E (1998) Detection of shallow objects using refracted and diffracted seismic waves. J Appl Geophys 38:155–168

Betchel National, Inc (1984a) The geology and hydrogeology of Bear Creek Valley waste disposal areas A and B, May, 1984. Oak Ridge National Laboratory Report Y/SUB/84-47974C/3

Betchel National, Inc (1984b) Interim report on the geology and hydrogeology of the southern and western perimeter to the Burial Grounds and the interior portions of Bear Creek Valley waste disposal areas environmental field studies, May 1984. Oak Ridge National Laboratory Report Y/SUB/84-47974C/4

Betchel National, Inc (1984c) Geologic data on twenty monitoring wells installed in Bear Creek valley in September and October 1984, Oak Ridge Y-12 Plant. Oak Ridge National Laboratory Report Y/SUB/84-47974C/12

Carpenter PJ, Doll WE, Kaufmann RD (1995) Geophysical surveys over karst features near Oak Ridge Y-12 plant, Oak Ridge, Tennessee. Oak Ridge National Laboratory Report Y/ER-200

Carpenter PJ, Doll WE, Kaufmann RD (1998) Geophysical character of buried sinkholes on the Oak Ridge Reservation, Tennessee. J Environ Eng Geophys 3:133–145

Carpenter PJ, Higuera-Diaz IC, Thompson MD, Atre S, Mandell W (2003) Accuracy of seismic refraction tomography codes at karst sites. In: SAGEEP03: symposium on the application of geophysics to engineering and environmental problems. Environmental and Engineering Geophysical Society, Wheat Ridge, CO, pp 832–840 (CD-ROM)

Chen J, Hubbard S, Peterson J, Williams K, Fienen M, Jardine P, Watson D (2006) Development of a joint hydrogeophysical inversion approach to a contaminated fractured aquifer. Water Resour Res 42 (paper W06425)

De Amorim WN, Hubral P, Tygel M (1987) Computing field statics with the help of seismic tomography. Geophys Prospect 35:907–919

Docherty P (1992) Solving for the thickness and velocity of the weathering layer using 2-D refraction tomography. Geophysics 57:1307–1318

Doll WE (1998) Reprocessing of shallow seismic reflection data to image faults near a hazardous waste site on the Oak Ridge Reservation, Tennessee. In: SAGEEP98: Symposium on the application of geophysics to engineering and environmental problems. Environmental and Engineering Geophysical Society, Wheat Ridge, CO, pp 705–714

Doll WE, Carr BJ, Sheehan JR, Mandell WA (2005) Overview of karst effects and karst detection in seismic data from the Oak Ridge Reservation, Tennessee. In: Kuniansky EL (ed) U.S. Geological Survey Karst Interest Group Proceedings, Rapid City, SD, U.S. Geological survey scientific investigations report SIR 2005-5160, pp 20–28. http://pubs.usgs.gov/sir/2005/5160

Dreier RB, Caldanaro AJ (1994) Installation summary for the DNAPL characterization multiport wells, GW-726, GW-727, GW-729, GW-730 and GW-790. Y-12 Plant Environmental Restoration Report Y/ER-117, Oak Ridge, p 47

Dreier RB, Haase CS, Beaudoin CM, King HL, Switek J (1987) Summary of geological data in the vicinity of the hydrofracture facilities. Oak Ridge National Laboratory Report ORNL/RAP/LTR-87/26

Foreman JL, Dunne WM (1991) Conditions of vein formation in the southern Appalachian foreland: constraints from vein geometries and fluid inclusions. J Struct Geol 13:1173–1183

GeoTomo LLC (2001) GeoCT-I^{TM} automatic tomography software, version 1.2: advanced real-time automatic tomography for geophysical engineering applications, users guide and codes. Geo Tomo LLC, Houston, p 27

Geraghty and Miller, Inc (1985) Remedial alternative for Bear Creek Valley Waste Disposal Area. Oak Ridge Y-12 Plant Report Y/SUB/85-00206C/3

Goldstrand PM (1995) Stratigraphic variations and secondary porosity within Maynardville limestone in Bear Creek Valley, Y-12 Plant, Oak Ridge, Tennessee, Oak Ridge Y-12 Plant Report Y/TS-1093

Goldstrand PM, Shevenell LA (1997) Geologic controls on porosity development in the Maynardville Limestone, Oak Ridge, Tennessee. Environ Geol 31:248–258

Hatcher, RD Jr, Leminsky PJ, Drier RB, Ketelle RH, Lee RR, Leitzke DA, McMaster WM, Foreman JL, Lee SY (1992) Status report

on the geology of the Oak Ridge Reservation: Oak Ridge National Laboratory Report ORNL/TM-12074, p 244

Higuera-Diaz IC, Carpenter PJ, Thompson MD (2007) Identification of buried sinkholes using refraction tomography at Ft. Campbell Army Airfield, Kentucky. Environ Geol 53:805–812

Hollon DM (1997) The effect of fractures, faults, and sheared shale zones on the hydrology of Bear Creek Burial Grounds A-South, Oak Ridge, Tennessee. MS, Texas A & M University, College Station, p 161

Jones SB, Harrington BK, Field SM (1992) Updated subsurface data base for Bear Creek Valley, Chestnut Ridge, and parts of Bethel Valley on the U. S. Department of Energy, Oak Ridge Reservation, Oak Ridge Y-12 Plant. Oak Ridge Y-12 Plant Report Y/TS-881, p 208

King HL, Haase CS (1987) Subsurface-controlled geologic maps for the Y-12 Plant and adjacent areas of Bear Creek Valley. Oak Ridge National Laboratory Report ORNL/TM-10112

King HL, Haase CS (1988) Summary of results and preliminary interpretation of hydrogeologic packer testing in core holes GW-131 through GW-135 and CH-157, Oak RidgeY-12 Plant. Oak Ridge Y-12 Plant Report Y/TS-495, p 49

Leucci G (2003) Evaluation of karst stability using integrated geophysical methods. Geo Acta 2:75–88

Leucci G (2004) Evaluation of 2D resistivity and seismic refraction methods in a complex karstic area. Geo Acta 3:43–53

Moore GK (1988) Concepts of groundwater occurrence and flow near Oak Ridge National Laboratory, Tennessee. Oak Ridge National Laboratory Report ORNL/TM-10969, p 96

Sheehan JR, Doll WE, Mandel W (2005) An evaluation of methods and available software for seismic refraction tomography analysis. J Environ Eng Geophys 10:21–34

Shevenell L, Beauchamp J (1994) Evaluation of cavity occurrence in the Maynardville Limestone and Copper Ridge Dolomite at the Y-12 Plant using logistic and general linear models. Oak Ridge Y-12 Plant Report Y/TS-1022, p 43

Shevenell L, Dreier RB, Jago WK (1992) Summary of fiscal years 1991 and 1992 construction, hydrologic, and geological data obtained from the Maynardville Limestone Exit Pathway Monitoring Program. Oak Ridge Y-12 Plant Report Y/TS-814, p 144

Sledz JJ, Huff DD (1981) Computer model for determining fracture porosity and permeability in the Conasauga Group. Oak Ridge National Laboratory Report ORNL/TM-7695

Solomon DK, Moore GK, Toran LE, Drier TB, Mccaster WM (1992) Status report: a hydrologic framework for the Oak Ridge Reservation. Oak Ridge National Laboratory Report ORNL/TM-12026

Thompson MD (1995) Seisx: Seismic trace plotting and picking program, MS-DOS version (codes and documentation). MDT Associates, Bolingbrook, IL, p 3

Zhang J, Toksöz MN (1998) Nonlinear refraction travel time tomography. Geophysics 63:1726–1737

Zhang J, ten Brink U, Toksoz MN (1998) Nonlinear refraction and reflection travel-time tomography. J Geophys Res 103:29743–29757

Zhu X, Sixta DP, Angstman BG (1992) Tomostatics, turning ray tomography + static corrections. Leading Edge 11:15–23